

Raman resonances mediated by excitonic polarons in BiVO_4

Georgy Gordeev,^{1,2,*} Christina Hill,^{1,2,3} Angelina

Gudima,¹ Stephanie Reich,⁴ and Mael Guennou¹

¹*Department of Physics and Materials Science, University of Luxembourg,
30 avenue des Hauts-Fourneaux, 4362 Esch-sur-Alzette, Luxembourg*

²*Inter-institutional Research Group Uni.lu–LIST on Ferroic
Materials, 41 rue du Brill, L-4422 Belvaux, Luxembourg*

³*Materials Research and Technology Department, Luxembourg Institute
of Science and Technology, 41 rue du Brill, L-4422 Belvaux, Luxembourg*

⁴*Department of Physics, Freie Universität Berlin, Arnimallee 14, 14195 Berlin*

(Dated: March 25, 2026)

Abstract

Excitonic polarons are quasiparticles formed by a Coulomb-bound electron-hole pair with strong coupling to lattice vibrations. Despite high fundamental interest in excitonic polarons, the experimental investigation of these particles remains challenging. In this work, we exploit the resonant Raman effect to probe the excitonic polarons in bismuth vanadate. We track enhancement of Raman modes as a function of excitation energy and reveal two optical resonances: one inside the band gap at 1.94 eV and another one near the optical absorption edge at 2.45 eV. The high-energy resonance originates from free excitons, which exhibit a characteristic 40 meV anisotropy between polarizations parallel and perpendicular to the c axis. Remarkably, the low-energy resonance shows no contrast in the optical absorption spectra. We attribute this resonance to an excitonic polaron formed through strong exciton-phonon coupling, making excitonic and excitonic-polaron Raman resonances similar in strength. We probe the energy level of the excitonic polaron and compare its coupling strength to the different vibrational modes. Our results establish resonant Raman spectroscopy as a unique and powerful tool for probing quasiparticles of polaronic and excitonic nature in oxide materials.

A bound electron-hole pair forms an exciton, a neutral quasiparticle that modifies the absorption band-edge. When either an electron or a hole attracts a local phonon cloud, a polaron is formed, altering transport phenomena.^{1,2} Remarkably, a simultaneous strong interaction between an exciton and a phonon results in an excitonic polaron (EP).³⁻⁶ The EP intertwines optical and electrical transport properties, relevant for photo-catalysis and photo-voltaic applications.^{5,7} Despite tremendous interest, the unambiguous detection of EPs remains challenging. Most works focus on the emission properties, where strong exciton-phonon coupling produces a new emission line labeled as a self-trapped exciton (STE).⁶ The emission of EPs is dominated by the post-absorption relaxation processes and is often represented by a broad emission peak associated with a significant Stokes shift.⁸⁻¹² The Stokes-shifted emission however, can be confused with other phenomena and does not directly yield EP key characteristics, such as formation energy,^{7,13,14} formation lifetime, and phonon modes that participate in EP formation. Novel experimental methods sensitive to exciton-phonon coupling are necessary to capture the EP formation and resolve the phonon branches dressing EPs.

Monoclinic bismuth vanadate (BiVO_4) is a well-established host for excitons¹⁵ and polarons.^{7,13,14,16–18} It has been shown that excess holes preferentially form polarons that are delocalized across multiple lattice sites^{7,16,19}, classifying them as large polarons. These large hole polarons exhibit moderate drift mobility under electric field. In contrast, excess electrons are likely to form polarons that are highly localized within a single unit cell, referred to as small polarons.^{7,14,20,21} Due to their strong localization, these small electron polarons have extremely low mobility and significantly reduce the charge carrier conductivity of BiVO_4 . The optical absorption edge¹⁵ in BiVO_4 is dominantly defined by excitons, and these excitonic effects remain substantial up to room temperatures.²² The coexistence of strong Coulomb interactions and significant coupling to lattice vibrations suggests the formation of excitonic polarons, verified both experimentally²³ and computationally¹². With an optical absorption edge in the visible light range at approximately 2.50 eV²⁴, the various excitonic and polaronic states become relevant for solar-light photo-induced effects. This makes BiVO_4 an ideal candidate for identifying and characterizing excitonic and polaronic states via resonant Raman spectroscopy.

In this work, we implement resonant Raman scattering to investigate excitonic polarons in BiVO_4 . The A_g modes are excited with 16 laser energies, across and below the band gap. We measure the Raman cross-section as a function of excitation energy. Resonances occur when the excitation approaches either the optical band gap or a new in-gap transition. We discuss the origin of the in-gap resonance and attribute it to the excitonic polaron. Notably, this EP transition is invisible in linear optical absorption but reappears at a different energy in form of emission from a self-trapped exciton. Finally, we discuss the nature and the properties of the observed EP and establish its new distinctive signature, representing a strong Raman resonance accompanied by negligible optical absorption.

Results and discussion

At room temperature monoclinic BiVO_4 has a $C2/c$ symmetry with lattice parameters (in the non-standard $I2/a$ setting) $a = 5.186 \text{ \AA}$, $b = 5.084 \text{ \AA}$, and $c = 11.69 \text{ \AA}$, $\gamma = 89.61^\circ$.^{25,26} The Raman-active vibrations of BiVO_4 are well characterized experimentally^{27,28} and have been identified through DFT calculations.²⁸ Group-theory analysis predicts 18 Raman-active modes, consisting of 8 modes of A_g symmetry and 10 modes of B_g symmetry. In this work, we focus on the A_g modes; they are activated when the incident and scattered polarization

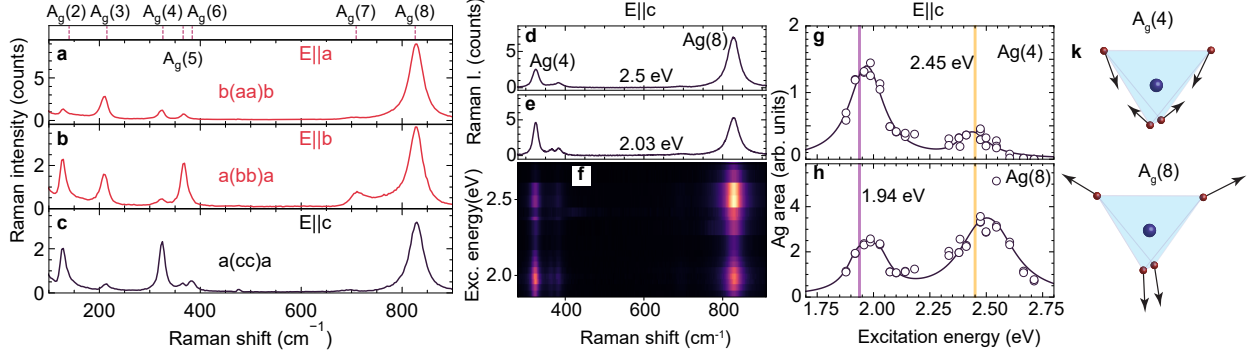


FIG. 1. Resonant Raman spectroscopy applied to the BiVO_4 single crystal. Raman spectra acquired with 2.3 eV excitation for incident and scattered photons polarized along **a** $E||a$, **b** $E||b$, and **c** $E||c$. A_g modes with $E||c$ **d** excited near the band gap energy at 2.5 eV and **e** inside the gap at 2.03 eV. **f** Resonant Raman map measured with $E||c$. Resonant Raman profile of **g** the $A_g(4)$ and **h** the $A_g(8)$ mode, where symbols represent experimental data and solid lines are fits using Eqs. S1 and S2. Vertical lines indicate the optical transition energies extracted from the fit. **k** Eigenvectors of the $A_g(8)$ mode and $A_g(4)$ mode within a VO_4 tetrahedron.

are aligned. The A_g modes originate from the motion of oxygen and vanadium atoms, where small polarons form.¹³ Figure 1a–c shows the Raman spectra of BiVO_4 for light polarized along three different crystallographic directions. Among all A_g modes, the $A_g(8)$ mode at approximately 826 cm^{-1} exhibits the strongest intensity in all three polarization configurations. In the following, we focus on $A_g(8)$ and $A_g(4)$ modes because of its dominant intensity and strong polarization-dependent Raman response. For instance, the $A_g(4)$ mode at 326 cm^{-1} becomes comparably strong for the electric field of the laser light E oscillating $\parallel c$, corresponding to $a(cc)a$ in Porto’s notation, as shown in Figure 1c.

Raman resonances of the optical many-body states. At first, we study in detail the optical resonances for case when $E \parallel c$. Two Raman spectra are exemplified in Figure 1d and 1e, excited with 2.50 and 2.03 eV, respectively. In this polarization configuration, the $A_g(8)$ and $A_g(4)$ modes exhibit the strongest intensities. The intensity ratio of these two modes varies with the excitation energy. At 2.03 eV, their amplitudes are almost equal, whereas at 2.50 eV the $A_g(8)$ mode dominates. The systematic variation in Raman intensity as a function of excitation energy is most evident in a two-dimensional resonant Raman

map shown in Figure 1f. In this map, the vertical axis represents the excitation energy, whereas the horizontal axis corresponds to the Raman shift, and the color scales with Raman intensity. Data were collected using 16 laser energies ranging from 1.87 to 2.71 eV. The $A_g(4)$ and the $A_g(8)$ modes are primarily visible. Along the excitation-energy axis, two maxima appear in the high- and low-energy ranges, signaling the presence of two optical resonances at approximately 2.0 eV and 2.5 eV.

The two observed Raman resonances yield a similar intensity despite different underlying nature of optical transitions. We quantify their parameters using resonant Raman profiles shown in Figure 1g. In such a profile, the y-axis represents the Raman cross section of the investigated Raman mode, while the x-axis corresponds to the excitation energy. Figure 1g shows the resonant Raman profile of the $A_g(4)$ mode, displaying two resonances at which $A_g(4)$ peak area reaches its maximum. The data fits by Eqs. S1 and S2 and represented by the solid line in Figure 1g. The model yields two optical transitions energies at 2.40 eV and 1.94 eV. We systematically observe two resonances near these energies in all profiles of the A_g shown in Figure S2. The high-energy resonance occurs at the absorption edge²⁹ and can be attributed to free delocalized exciton (FE). However the low-energy resonance at 1.94 eV is non-trivial and occurs well inside the gap. It may be preliminarily attributed to the EP state. To confirm this interpretation we next compare the optical response of two resonances and their coupling strength to different phonon modes.

The small polaron wavefunction is confined within the VO_4 tetrahedron,¹³ such that the local symmetry of the vibrational modes governs the coupling strength. While the $A_g(4)$ mode responds strongly to the low-energy optical transition, the resonant Raman profile of the $A_g(8)$ mode shows a stronger resonance for the high-energy optical transition, see Figure 1h. These modes correspond to the motion of oxygen atoms within the different local symmetry. Locally, the $A_g(8)$ mode appears to be fully symmetric, see Figure 1k. All four oxygen atoms perform breathing-like vibrations by symmetrically changing only the V-O bonds length, inducing non-polar vibration. In contrast, the $A_g(4)$ mode has more of a bending-like character, with two top and bottom oxygen atoms moving upwards and downwards simultaneously, where the angles between the V-O bonds change, see eigenvectors in Figure 1k. We believe that a distinct vibrational character of the $A_g(4)$ mode causes a different resonant Raman response compared to the $A_g(8)$ mode. Thus, resonant Raman profiles efficiently compare coupling to phonons of the excitonic and EP states. We can

further analyze EP-photon coupling strength using linear optical spectroscopy.

Optical response of free excitons and excitonic polarons. We carry out linear optical spectroscopy to investigate the high- and low-energy Raman resonances. We quantify the optical gaps using the Tauc plot shown in Figure 2a, where $(\alpha\hbar\omega)^n$ is plotted versus $\hbar\omega$. We choose $n = 2$ which is most appropriate for direct allowed interband transitions in crystalline materials.³⁰ The absorption coefficient α is calculated as $\frac{1}{d}\log(\frac{1-R}{T})$. The linear fit to $\alpha = 0$ yields an optical gap $E_{opt}^c = 2.47$ eV for $E||c$ and $E_{opt}^{a,b} = 2.35 \pm 0.02$ for $E \perp c$, with an optical anisotropy of approximately 120 meV, similar to previous reports that rely on linear optics.^{15,24,29} However Tauc plots are limited in terms of absolute numbers and overestimate the anisotropy of the band gap.³⁰ The gap anisotropy is measured more accurately by resonant Raman spectroscopy and yields 40 meV, see Figure 2b. The energy of the optical gaps matches the high-energy resonances at 2.45 eV for $E||c$ and at 2.41 eV for $E \perp c$, as shown in Figure 2b. The anisotropic optical band gap near 2.41 eV is confirmed to be the free exciton, remaining bound at room temperature.^{15,23} The FE manifest regularly in optical and resonant Raman spectroscopies: it shapes the absorption band-edge and producing the Raman resonance at the same energy.

We now test the nature of the EP resonance at 1.94 eV, finding several observations consistent with our interpretation. Compared to the FE it is practically undetectable in linear optical spectroscopy, see purple line in Figure 2a. We as well find no signature in the reflectivity spectra shown in Figure S3. Indeed the interaction of EP with light is expected to be weak since the EP state is highly localized and energetically narrow.⁶ Another important aspect is the exceptionally strong EP-phonon coupling observed in the resonant Raman profiles that have similar intensity with FE Raman resonances. The Raman intensity scales as $M_{EP-photon}^4$ and $M_{EP-phonon}^2$, where M is the matrix element in SEq. (2). It requires quadratically stronger EP-phonon coupling to compensate the for weak EP interaction with photons and produce Raman resonances of comparable strength. Indeed, a strong EP-phonon coupling is expected for the EP formation, where charges are dressed by a phonon cloud.

The observed EP state is most likely formed by a localized electron polaron and a delocalized hole from the valence band. In BiVO₄, electron polarons are expected to lie between 0.3 eV^{14,21}, 0.5 eV¹³ and 0.88 eV⁷ below the conduction band, which coincides with the en-

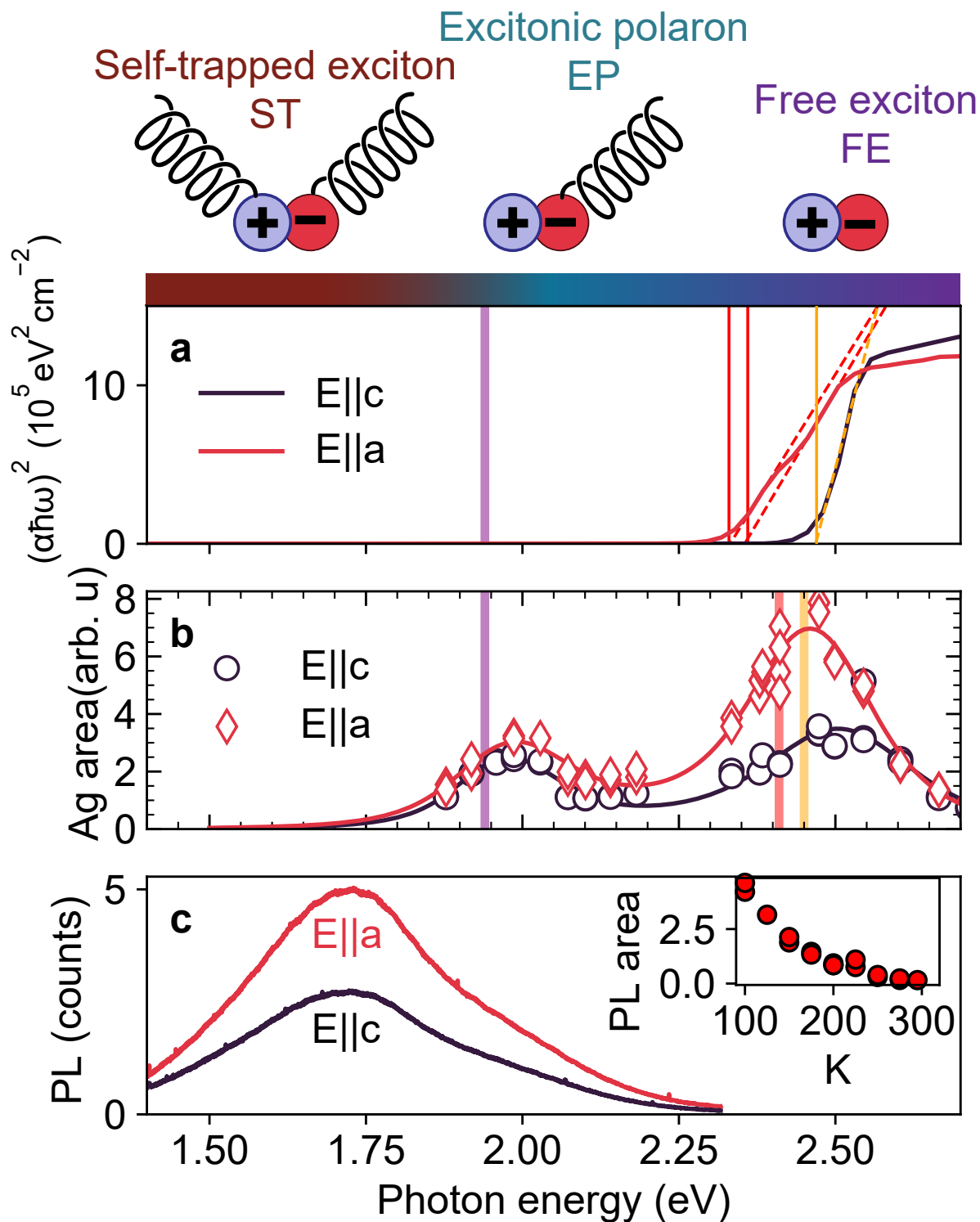


FIG. 2. Optical signatures of excitonic and EP states. **a** Tauc plot showing anisotropy of the optical absorption edges for light polarized along the crystallographic c and a axes. **b** Resonant Raman profiles of the $A_g(8)$. The yellow (red) vertical line indicates the transition energy of free excitons for $E||c$ ($E||a$) in the energy range of the optical band gap. The vertical purple line marks the energy of the EP state, which is only observed in resonant Raman spectroscopy. **c** Photoluminescence from self-trapped excitons with the maximum at 1.74 eV excited with a 2.8 eV

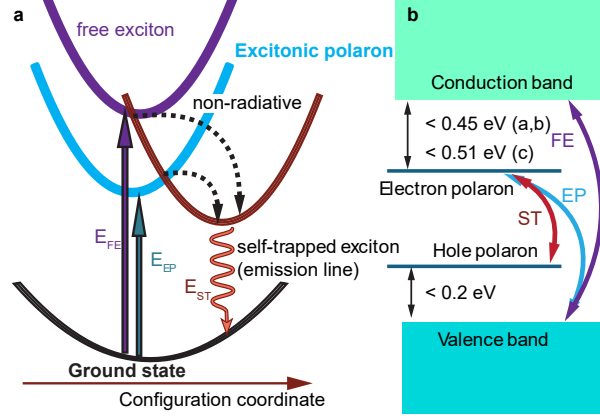


FIG. 3. Energy level diagram and formation energies of EP. **a** Many-body picture with free excitons (purple), excitonic polarons (blue), and self-trapped excitonic states (red) in BiVO_4 . Direct up-pointing arrows indicate optical absorption, tilted arrows indicate non-radiative scattering, and the wavy arrow represents the emission from the self-trapped excitonic state into the ground state. **b** Energy diagram with the in-gap energy levels of electron and hole polarons in BiVO_4 .

ergy region where we observe the lower-energy Raman resonance. A hole-based EP, where localized hole couples to a delocalized electron, can be excluded because hole polarons are predicted to lie only ≈ 100 meV^{7,16,19,31} above the valence band, far too deep inside the band gap compared to the experimental resonance energy. In addition, the expansion of hole polarons in monoclinic BiVO_4 is large compared to the unit cell. The EP-phonon coupling for large polarons is predicted to be small at the Γ point, where the Raman process occurs.⁶ Another possible origin could be a defect-induced state, but in BiVO_4 , point defects such as oxygen vacancies have been shown to lead to the formation of polarons.^{32–34}

While hole-polarons weakly contribute to Raman scattering they can still form self-trapped excitons via finite momentum phonons, defining new photoluminescence line (PL). We therefore take a closer look at the emission properties of the BiVO_4 crystal. In Figure 2c we show the PL emission peaking at 1.74 eV. Previously, this emission has been attributed to the defect-bound excitons, yet it's intensity is almost insensitive to hydrogen passivation.³⁵ Instead, we interpret this as a classical self-trapped exciton: its emission has a Stokes shift compared to EP and FE states. The emission intensity increases at low temperature, see the inset in Figure 2c, consistent with self-trapped exciton interpretation and previous reports in thin films.³⁵ The lattice trapping is more stable at low temperatures and higher STE

emission is expected. Further, the full width at half maximum of this peak is twice as broad 0.5 eV as for the EP and FE states with 0.2-0.3 eV, caused by the finite-momentum phonons, another key property of the self-trapped excitons. In BiVO₄ it is clearly apparent that the EP and self-trapped excitons represent two distinct states, despite both being formed by a strong exciton-phonon coupling.

Formation energies of many-body states in BiVO₄. Figure 3a visualizes the optical absorption into free excitons and excitonic polarons while the emission occurs from the self-trapped excitonic states. From our resonant Raman and the PL measurements we can estimate the upper bound of hole- and electron-polarons formation energies ΔH_f , assuming that the electron-hole binding energy of the localized EP states exceeds the binding energy of delocalized FE.³⁶ In the main crystallographic directions, we find the same EP energy E_{EP} 1.94 eV, see purple line in Figure 2a,b. The electron-polaron formation energy is estimated as $\Delta H_{f,el-pol} < (E_{FE} - E_{EP})$. For the c axis we find $\Delta H_{f,el-pol}^c < 0.51$ eV, whereas for the a,b axes we find $\Delta H_{f,el-pol}^{a,b} < 0.45$ eV, see Figure 3b. These values approach well the first-principles calculations from Kweon *et al.*^[14] and Pham and Deskins^[13]. Anisotropic electron-polaron hopping is driven by the variation of the formation energy and is more probable towards a, c directions, as previously reported by facet-selective charge accumulation.³⁷⁻³⁹ Similarly, we can estimate the upper limit for the hole-polaron formation energy $\Delta H_{f,hole-pol}$ by $(E_{EP} - E_{ST})$. The energy of the hole-polaron can be found at 0.2 eV above the valence band, see Figure 3b.

In summary, we implemented resonant Raman spectroscopy as a unique tool to distinguish and measure excitonic polarons. The polarization-resolved Raman profiles of the A_g modes in BiVO₄ reveal two well-separated resonances: a high-energy feature at 2.41–2.45 eV, associated with free excitons and tracking the anisotropic optical absorption edge (40 meV), and a sub-gap resonance at 1.94 eV, which we assign to excitonic polarons enabled by strong EP–phonon coupling. These findings demonstrate that resonant Raman spectroscopy provides direct and selective fingerprints of excitonic polaron formation, offering an experimental bridge to emerging theoretical descriptions.^{5,6} Beyond this system, EP-mediated Raman processes enable access to a broad class of polaronic quasiparticles, including defect-bound⁴⁰, spin⁴¹, and surface polarons⁴². Resonant Raman spectroscopy thus emerges as a powerful and versatile probe of polaronic excitations in semiconducting oxides.

Data availability

The data were deposited online and will be published after the embargo period. DOI 10.5281/zenodo.18679516

Methods

Sample. For this purpose, we used a single crystal purchased from SurfaceNet GmbH and grown by the Czochralski method.

Raman spectroscopy. The Raman measurements were done on a Horiba T64000 microspectrometer with Rayleigh light rejected by long-pass filters and Raman signal dispersed by 900 grooves per mm grating. The laser light was produced by a Coherent 70C Ar-Kr and Radiant Dye dye lasers. The spectral intensities are normalized to the A_g mode of a CaF_2 crystal, which exhibits a constant Raman cross section in the visible wavelength range.

UV-Vis spectroscopy. Reflectivity and transmission were measured in 5 nm steps with light polarized parallel and perpendicular to the c axis using a Lambda 1050+ uv/vis/nir Perkin-Elmer spectrometer; see Figure S3.

Photoluminescence. The sample was excited with a He-Cd 441.3 nm laser line and re-emitted light collected and processed with a Renishaw spectrometer, equipped with 300 grooves per nm grating and Silicon CCD. For cryogenic temperatures, an Oxford Instruments Microstat was used.

Acknowledgments

GG, MG, and CH acknowledge funding from the Fond National de la Recherche under Project PRIDE/15/10935404. This research was funded in whole, or in part, by the Luxembourg National Research Fund (FNR), grant reference [INTER/MERA20/14995416/SWIPE/AWORD]. For the purpose of open access, and in fulfillment of the obligations arising from the grant agreement, the author has applied a Creative Commons Attribution 4.0 International (CC BY 4.0) license to any Author Accepted Manuscript version arising from this submission. The authors are grateful to J. Iniguez, H-J Zhao, D. Vincent and X. Rocquefelte for preliminary calculations of BiVO_4 phonon modes and eigenvectors.

* georgy.gordeev@uni.lu

- [1] I. Austin and N. Mott, Polarons in crystalline and non-crystalline materials, *Advances in Physics* **18**, 41 (1969).
- [2] A. Bosman and H. van Daal, Small-polaron versus band conduction in some transition-metal oxides, *Advances in Physics* **19**, 1 (1970).
- [3] Y. Toyozawa and J. Hermanson, Exciton-phonon bound state: A new quasiparticle, *Physical Review Letters* **21**, 1637 (1968).
- [4] G. Iadonisi and F. Bassani, Excitonic polaron states and optical transitions, *Il Nuovo Cimento D* **2**, 1541 (1983).
- [5] Z. Dai, C. Lian, J. Lafuente-Bartolome, and F. Giustino, Excitonic polarons and self-trapped excitons from first-principles exciton-phonon couplings, *Physical Review Letters* **132**, 036902 (2024).
- [6] Z. Dai, C. Lian, J. Lafuente-Bartolome, and F. Giustino, Theory of excitonic polarons: From models to first-principles calculations, *Physical Review B* **109**, 045202 (2024).
- [7] J. Wiktor, F. Ambrosio, and A. Pasquarello, Role of polarons in water splitting: The case of BiVO₄, *ACS Energy Letters* **3**, 1693 (2018).
- [8] S. Li, J. Luo, J. Liu, and J. Tang, Self-trapped excitons in all-inorganic halide perovskites: Fundamentals, status, and potential applications, *The Journal of Physical Chemistry Letters* **10**, 1999.
- [9] J. Li, H. Wang, and D. Li, Self-trapped excitons in two-dimensional perovskites, *Frontiers of Optoelectronics* **13**, 225 (2020).
- [10] A. Abfaltrerer, J. Shamsi, D. J. Kubicki, C. N. Savory, J. Xiao, G. Divitini, W. Li, S. Macpherson, K. Galkowski, J. L. MacManus-Driscoll, D. O. Scanlon, and S. D. Stranks, Colloidal synthesis and optical properties of perovskite-inspired cesium zirconium halide nanocrystals, *ACS Materials Letters* **2**, 1644 (2020).
- [11] Y. Bai, S. Zhang, N. Luo, B. Zou, and R. Zeng, Temperature-dependent self-trapped exciton emission in Cu(I) doped zinc-based metal halides from well-resolved excited state structures, *Nano Research* **17**, 7768 (2024).

- [12] T. Möslinger, N. Österbacka, and J. Wiktor, Competing self-trapped exciton states and multiple emission pathways in BiVO_4 , *The Journal of Physical Chemistry Letters* **16**, 6861 (2025).
- [13] T. D. Pham and N. A. Deskins, Efficient method for modeling polarons using electronic structure methods, *Journal of Chemical Theory and Computation* **16**, 5264 (2020).
- [14] K. E. Kweon, G. S. Hwang, J. Kim, S. Kim, and S. Kim, Electron small polarons and their transport in bismuth vanadate: A first principles study, *Physical Chemistry Chemical Physics* **17**, 256 (2015).
- [15] T. Das, X. Rocquefelte, R. Laskowski, L. Lajaunie, S. Jobic, P. Blaha, and K. Schwarz, Investigation of the optical and excitonic properties of the visible light-driven photocatalytic BiVO_4 material, *Chemistry of Materials* **29**, 3380 (2017).
- [16] K. E. Kweon and G. S. Hwang, Structural phase-dependent hole localization and transport in bismuth vanadate, *Physical Review B - Condensed Matter and Materials Physics* **87**, 205202 (2013).
- [17] T. Liu, Q. Zhao, C. Li, Y. Lyu, and M. Dupuis, Photocatalytic facet selectivity in BiVO_4 nanoparticles: Polaron electronic structure and thermodynamic stability considerations for photocatalysis, *Journal of Physical Chemistry C* **123**, 20142 (2019).
- [18] T. Liu, X. Zhou, M. Dupuis, and C. Li, The nature of photogenerated charge separation among different crystal facets of BiVO_4 studied by density functional theory, *Physical Chemistry Chemical Physics* **17**, 23503 (2015).
- [19] T. Liu, M. Cui, and M. Dupuis, Hole polaron transport in bismuth vanadate BiVO_4 from hybrid density functional theory, *The Journal of Physical Chemistry C* **124**, 23038 (2020).
- [20] N. Aiga, Q. Jia, K. Watanabe, A. Kudo, T. Sugimoto, and Y. Matsumoto, Electron-phonon coupling dynamics at oxygen evolution sites of visible-light-driven photocatalyst: Bismuth vanadate, *The Journal of Physical Chemistry C* **117**, 9881 (2013).
- [21] A. J. E. Rettie, W. D. Chemelewski, D. Emin, and C. B. Mullins, Unravelling small-polaron transport in metal oxide photoelectrodes, *The Journal of Physical Chemistry Letters* **7**, 471 (2016).
- [22] J. Wiktor, I. Reshetnyak, F. Ambrosio, and A. Pasquarello, Comprehensive modeling of the band gap and absorption spectrum of BiVO_4 , *Physical Review Materials* **1**, 022401 (2017), publisher: American Physical Society.

- [23] J. Zhang, J. Shi, Y. Chen, K. H. Zhang, and Y. Yang, Bimolecular self-trapped exciton formation in bismuth vanadate, *Journal of Physical Chemistry Letters* **13**, 9815 (2022).
- [24] J. K. Cooper, S. Gul, F. M. Toma, L. Chen, Y.-S. Liu, J. Guo, J. W. Ager, J. Yano, and I. D. Sharp, Indirect bandgap and optical properties of monoclinic bismuth vanadate, *The Journal of Physical Chemistry C* **119**, 2969 (2015).
- [25] R. S. Roth and J. L. Waring, Synthesis and stability of bismutotantalite, stibiotantalite and chemically similar ABO_4 compounds, *American Mineralogist* **48**, 1348 (1963).
- [26] S. H. Choh and M. S. Jang, Domain structure and magnetic resonance studies of ferroelastic $BiVO_4$ revisited, *Materials Research Express* **3**, 045021 (2016).
- [27] L. P. Avakyants, A. V. Chervyakov, V. S. Gorelik, and P. P. Sverbil', Inelastic light scattering near the ferroelectric phase-transition point in bismuth vanadate crystals, *Journal of Russian Laser Research* **25**, 535.
- [28] J. Pellicer-Porres, D. Vázquez-Socorro, S. López-Moreno, A. Muñoz, P. Rodríguez-Hernández, D. Martínez-García, S. N. Achary, A. J. E. Rettie, and C. B. Mullins, Phase transition systematics in $BiVO_4$ by means of high-pressure-high-temperature raman experiments, *Physical Review B* **98**, 214109 (2018).
- [29] C. Hill, M. C. Weber, J. Lehmann, T. Leinen, M. Fiebig, J. Kreisel, and M. Guennou, Role of the ferroelastic strain in the optical absorption of $BiVO_4$, *APL Materials* **8**, 081108 (2020).
- [30] J. Klein, L. Kampermann, B. Mockenhaupt, M. Behrens, J. Strunk, and G. Bacher, Limitations of the tauc plot method, *Advanced Functional Materials* **33**, 2304523 (2023).
- [31] M. Ziwrtsch, S. Müller, H. Hempel, T. Unold, F. F. Abdi, R. van de Krol, D. Friedrich, and R. Eichberger, Direct time-resolved observation of carrier trapping and polaron conductivity in $bivo_4$, *ACS Energy Letters* **1**, 888 (2016), publisher: American Chemical Society.
- [32] N. Österbacka, F. Ambrosio, and J. Wiktor, Charge localization in defective $BiVO_4$, *The Journal of Physical Chemistry C* **126**, 2960 (2022).
- [33] T. W. Kim, Y. Ping, G. A. Galli, and K.-S. Choi, Simultaneous enhancements in photon absorption and charge transport of bismuth vanadate photoanodes for solar water splitting, *Nature Communications* **6**, 8769 (2015).
- [34] H. Seo, Y. Ping, and G. Galli, Role of point defects in enhancing the conductivity of $BiVO_4$, *Chemistry of Materials* **30**, 7793 (2018).

- [35] J. K. Cooper, S. B. Scott, Y. Ling, J. Yang, S. Hao, Y. Li, F. M. Toma, M. Stutzmann, K. V. Lakshmi, and I. D. Sharp, Role of hydrogen in defining the n-type character of BiVO₄ photoanodes, *Chemistry of Materials* **28**, 5761 (2016).
- [36] A. R. Kshirsagar and S. Reichardt, Understanding electronic excited states in BiFeO₃ via ab initio calculations and symmetry analysis, *Physical Review B* **110**, 155131 (2024).
- [37] R. Li, F. Zhang, D. Wang, J. Yang, M. Li, J. Zhu, X. Zhou, H. Han, and C. Li, Spatial separation of photogenerated electrons and holes among {010} and {110} crystal facets of BiVO₄, *Nature Communications* **4**, 1432 (2013).
- [38] G. Xi and J. Ye, Synthesis of bismuth vanadate nanoplates with exposed {001} facets and enhanced visible-light photocatalytic properties, *Chemical Communications* **46**, 1893 (2010).
- [39] D. Wang, H. Jiang, X. Zong, Q. Xu, Y. Ma, G. Li, and C. Li, Crystal facet dependence of water oxidation on BiVO₄ sheets under visible light irradiation, *Chemistry – A European Journal* **17**, 1275 (2011).
- [40] M. Setvin, C. Franchini, X. Hao, M. Schmid, A. Janotti, M. Kaltak, C. G. V. de Walle, G. Kresse, and U. Diebold, Direct view at excess electrons in TiO₂ rutile and anatase, *Physical Review Letters* **113**, 086402 (2014).
- [41] H. Y. Huang, Z. Y. Chen, R. P. Wang, F. M. F. de Groot, W. B. Wu, J. Okamoto, A. Chainani, A. Singh, Z. Y. Li, J. S. Zhou, H. T. Jeng, G. Y. Guo, J.-G. Park, L. H. Tjeng, C. T. Chen, and D. J. Huang, Jahn-teller distortion driven magnetic polarons in magnetite, *Nature Communications* **8**, 15929 (2017).
- [42] M. Kang, S. W. Jung, W. J. Shin, Y. Sohn, S. H. Ryu, T. K. Kim, M. Hoesch, and K. S. Kim, Holstein polaron in a valley-degenerate two-dimensional semiconductor, *Nature Materials* **17**, 676 (2018).

**Supporting information: Raman resonances mediated by
excitonic polarons in BiVO₄**

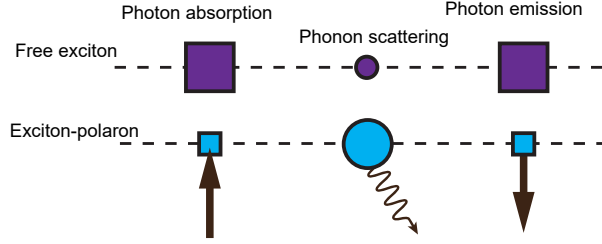
Georgy Gordeev,¹ Christina Hill,^{1,2} Angelina
Gudima,¹ Stephanie Reich,³ and Mael Guennou¹

¹*Department of Physics and Materials Science, University of Luxembourg,
30 avenue des Hauts-Fourneaux, 4362 Esch-sur-Alzette, Luxembourg*

²*Materials Research and Technology Department, Luxembourg Institute
of Science and Technology, 41 rue du Brill, L-4422 Belvaux, Luxembourg*

³*Freie Universität Berlin, Department of Physics, Arnimallee 14, 14195 Berlin*

(Dated: March 25, 2026)



Supporting Fig. 1. Scheme of resonant Raman scattering processes via exciton and exciton-polaron (EP). Vertical arrows are the photonic transitions and tilted arrows represent scattering by phonons.

RAMAN SCATTERING CROSS-SECTION

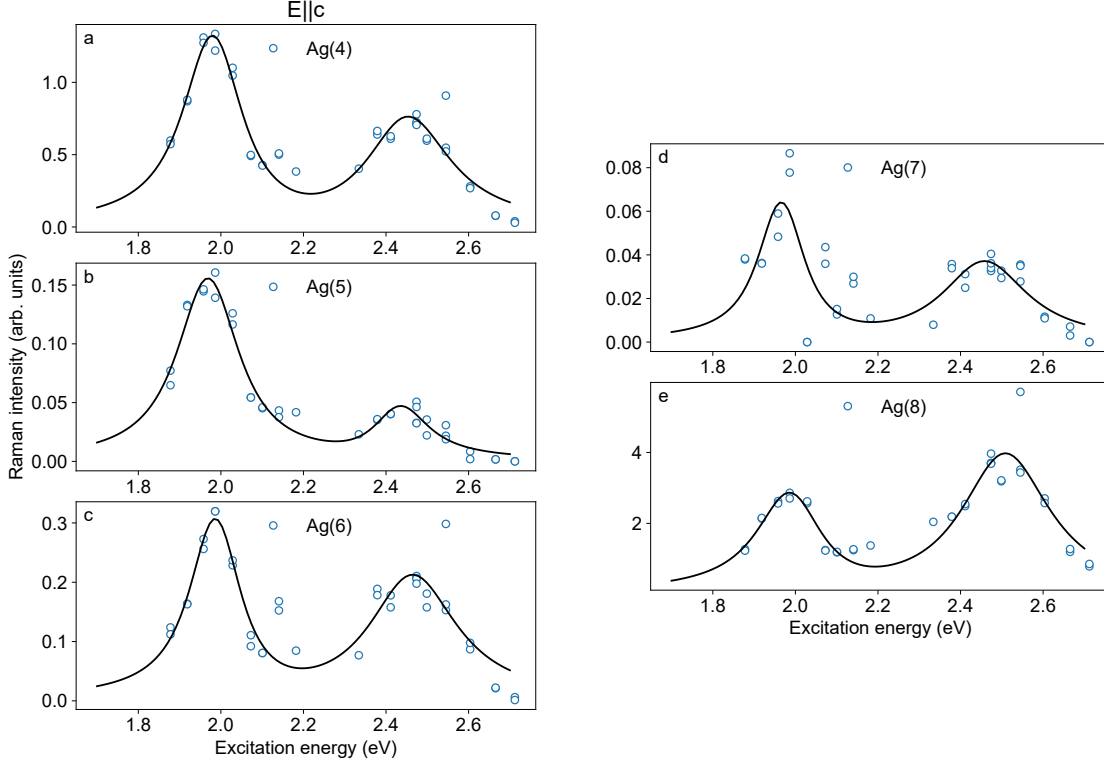
The Raman process mediated by the polaron is expected to have a superior cross-section. A Feynman diagram is depicted in Figure 1, where we illustrate a typical three-step Stokes Raman process. The visible light photon is first absorbed, then phonon is created followed by re-emission of the photon at a lower energy. The size of the vertex represents the interaction strength. For EP the interaction with the photon is weak, but it can be compensated by an enhanced EP-phonon scattering probability, since it is formed by the phonon interactions. The Feynman diagrams can be converted to a perturbation theory equation. We focus on symmetric A_g modes with dominant diagonal tensor elements, $R_{jj}^{A_g}$, with $j = a, b, c$. The wavelength dependence of $R_{jj}^{A_g}$ cross-section has contributions from FE and EP¹

$$R_{jj}^{A_g}(E_l) \propto E_l^4 |R_{jj}^{exc}(E_l) + R_{jj}^{EP}(E_l)|^2 \quad (1)$$

A contribution of a resonant state $R_{jj}^{exc,EP}$ is frequently described by the third-order perturbation theory, yielding dependence on laser energy E_l as¹

$$R_{i,jj}^{A_g}(E_l) = \frac{M_{photon-i,jj}^2 M_{i-ph}}{(E_l - E_i^{jj} - i\gamma_i)(E_l - E_i^{jj} - E_{ph} - i\gamma_i)}. \quad (2)$$

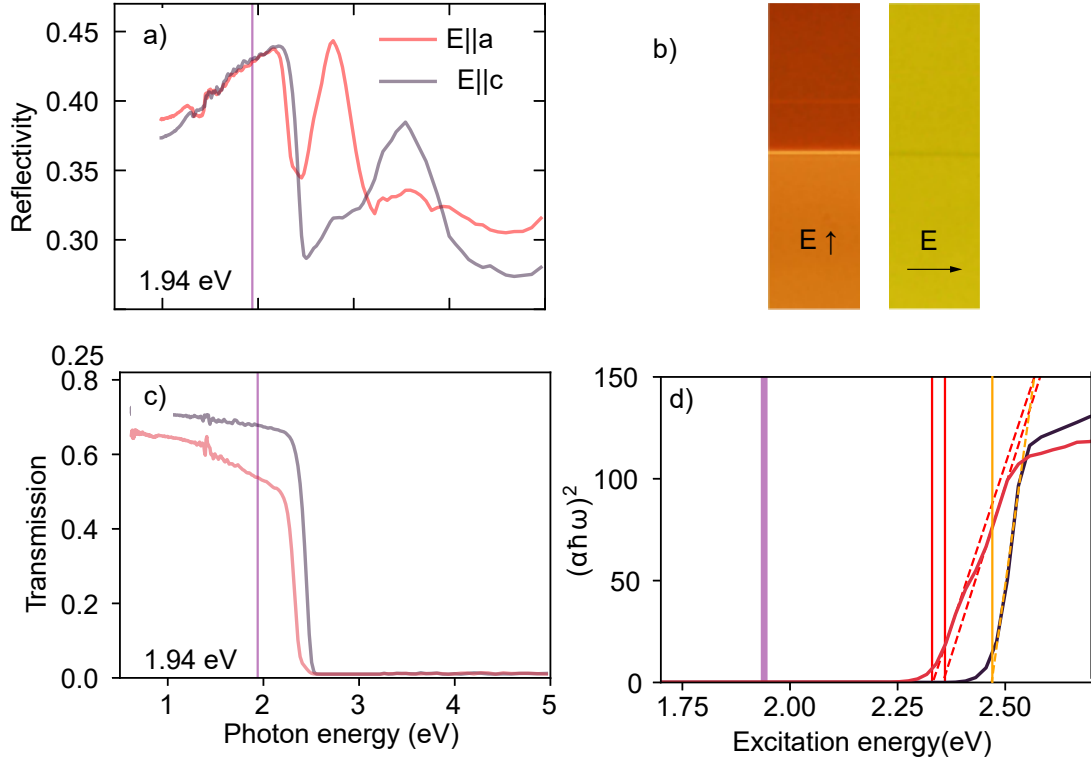
For excitons, where $i = exc, EP$, we find the matrix element $M_{photon-exc,jj}$ in the numerator that represents an interaction between an exciton and a photon, and j indicates polarization of the electric field oriented along a, b or c axis. M_{exc-ph} is the exciton-phonon matrix element. E_i^{jj} represents the energy of an exciton with a non-zero transition-dipole moment with light polarized along j . This energy matches the $E_{CB} - E_{VB} - E_B^{exc}$, E_B is the binding energy of the exciton, and E_{ph} is the energy of the phonon. The denominator contains so-called incoming and outgoing Raman resonances.



Supporting Fig. 2. Summary of the resonant Raman profiles from Ag modes excited in the $E \parallel c$ configuration

OPTICAL DATA

We now measure the linear optical properties of BiVO_4 to disentangle the contributions from the EP and exciton states. The optical spectra were measured in 5 nm steps with light polarized parallel and perpendicular to the c axis using a Lambda 1050+ uv/vis/nir Perkin-Elmer spectrometer, see Figure 3c. Anisotropy in the lowest optical band gap energies visible both in transmission and reflectivity spectra, shown in Figure 3a,b. We quantify the optical band gaps using Tauc plots shown in Figure 3c, where $(\alpha\hbar\omega)^n$ is plotted versus $\hbar\omega$. The absorption coefficient α is calculated as $\frac{1}{d}\log(\frac{1-R}{T})$. For fitting the Tauc plots, we choose $n = 2$, the most appropriate for crystalline materials.² The linear fit yields single energy for $E_{exc}^c = 2.47$ eV and two energies for $E \perp c$, $E_{exc}^{a,b} = 2.33$ and 2.37 eV, that correspond to a and b domains.³ These high-energy states manifest themselves in regular way both in optical absorption and resonant Raman, thus we confirm that the high-energy Raman resonance belongs to the excitonic state.



Supporting Fig. 3. Optical analysis of the anisotropy in BiVO_4 . (a) Reflectivity spectra with light polarized along and perpendicular to the c-axis. (b) Optical image of the sample in transmission mode. (c) Transmission spectra. (d) Tauc plots calculated from the transmission and reflectivity data.

-
- [1] P. Y. Yu and M. Cardona, *Fundamentals of Semiconductors – Physics and Materials Properties* (Springer, Berlin Heidelberg, 1995) pp. 18–83, arXiv:arXiv:1011.1669v3.
- [2] J. Klein, L. Kampermann, B. Mockenhaupt, M. Behrens, J. Strunk, and G. Bacher, Limitations of the tauc plot method, *Advanced Functional Materials* **33**, 2304523 (2023).
- [3] C. Hill, M. C. Weber, J. Lehmann, T. Leinen, M. Fiebig, J. Kreisel, and M. Guennou, Role of the ferroelastic strain in the optical absorption of BiVO_4 , *APL Materials* **8**, 081108 (2020).